HHS Public Access

Author manuscript

J Magn Reson Imaging. Author manuscript; available in PMC 2019 December 01.

Published in final edited form as:

J Magn Reson Imaging. 2018 December ; 48(6): 1551–1558. doi:10.1002/jmri.26012.

Value of Diffusion Kurtosis Imaging in Assessing Low-Grade Gliomas

Mohammed Z. Goryawala, Ph.D.[1], **Deborah O. Heros, M.D.**[2], **Ricardo J. Komotar, M.D.**[3], **Sulaiman Sheriff, B.S**[1], **Efrat Saraf-Lavi, M.D.**[1], and **Andrew A. Maudsley, Ph.D.**[1]

[1]Department of Radiology, University of Miami, Miami, FL, USA

[2]Department of Neurology, University of Miami, Miami, FL, USA

[3]Department of Neurological Surgery, University of Miami, Miami, FL, USA

Abstract

Background—Diffusion kurtosis imaging (DKI) measures have been shown to provide increased sensitivity relative to diffusion tensor imaging (DTI) in detecting pathologies.

Purpose—To compare the sensitivity of DKI derived kurtosis and diffusion maps for assessment of low-grade gliomas (LGG).

Study Type—Prospective study.

Population—19 LGG patients and 26 healthy control subjects were recruited.

Field Strength/Sequence—EPI diffusion-weighted MR images (b-values = 0, 1000, and 2000 with 30 diffusion gradient directions) were acquired on a 3T scanner.

Assessment—Maps for mean, axial and radial diffusivity (MD, AD, and RD) and kurtosis (MK, AK, and RK), and fractional anisotropy (FA) were evaluated in the tumor, perilesional white matter, and contralateral normal appearing white matter regions.

Statistical Testing—General linear models (GLM), Cohen's d for effect size estimates, false discovery rate (FDR) for multiple corrections, Cochran Q-test.

Results—Pairwise differences were observed for all diffusion and kurtosis measures between the studied regions (FDR $p < 0.001$), except FA map that failed to show significant differences between the lesion and pWM (FDR $p = 0.373$). Effect size analysis showed that kurtosis metrics were found to be 18.8% (RK, $p = 0.144$) to 29.1% (AK, $p < 0.05$) more sensitive in discriminating perilesional regions from the lesion than corresponding diffusion metrics, whereas AK provided a 25.0% ($p < 0.05$) increase in sensitivity in discriminating perilesional and contralateral white matter. RK was found to be the most sensitive to contralateral white matter differences between low-grade gliomas and controls, with MK and RK providing a significantly greater sensitivity of 587.2% ($p < 0.001$) and 320.7% ($p < 0.001$) than MD and RD, respectively.

*Corresponding Author: A. A. Maudsley, Ph.D., Department of Radiology, University of Miami School of Medicine, 1150 NW 14th St, Suite 713, Miami, FL 33136, Phone: 305-243-8080, Fax: 305-243-3405, AMaudsley@med.miami.edu.

Data Conclusion—Kurtosis maps showed increased sensitivity, as compared to counterpart diffusion maps, for evaluation of microstructural changes in gliomas with a 3–6 fold increment in assessing changes in contralateral white matter.

Keywords

diffusion kurtosis imaging; low-grade glioma; perilesional white matter; diffusion tensor imaging

INTRODUCTION

Measurement of water diffusion in brain tissue has been shown to provide valuable information for clinical diagnostic studies (1). The extension of these methods to map the tensor of the diffusion allows a direct examination of anisotropic aspects of tissue microstructure (2). The assumption of a Gaussian distribution of the water diffusion, however, presents a simplified model that does not fully characterize the diffusion within biological tissues (3). DKI is an expansion of DTI where a kurtosis tensor is estimated that has shown to be useful in characterizing the degree of non-Gaussian distribution of diffusion in biological tissue (4). This technique provides additional diffusion parameters relative to DTI (5) and values of kurtosis have been shown to be useful to quantify the complexity of tissue barriers (6). DKI measures have been shown to provide increased sensitivity and specificity in detecting pathological changes in ischemia (7), traumatic brain injury (8), Alzheimer's disease (9), and Parkinson's disease (10) relative to conventional diffusion weighted imaging (DWI) and diffusion tensor imaging (DTI) and has been shown to improve tumor grading in gliomas (11–13).

Infiltration of gliomas in the absence of changes on structural MR images has been reported (14,15), which complicates resection and reduces the efficacy of local radiation therapy (16). There is therefore considerable interest in imaging measurements that may increase sensitivity to detection of tumor infiltration in regions beyond the MR visible boundaries of gliomas in order to provide a more complete assessment of the disease and potentially improve prognosis.

Diffusion tensor imaging metrics have been shown to be most sensitive to changes of white matter architecture on a microscopic level and useful towards mapping of early invasive neuronal changes as a result of low-grade gliomas (17). The value of DKI for tumor grading has also been previously reported using measures in solid tumor region; however, few of these studies have studied microstructural changes in low grade gliomas (LGGs) in the perilesional space and the contralateral normal appearing white matter.

Studies using DWI and DTI have shown changes in the contralateral normal appearing white matter (cNAWM) in subjects with high-grade gliomas, with increased mean diffusivity (MD) and decreased fractional anisotropy (FA) (18–20). In a previous study, we showed that increased MD in cNAWM was associated with altered metabolite levels (21). Further, DTI has been also shown to be useful in monitoring radiation-induced demyelination and mild structural degradation of axonal fibers after radiation therapy and has been postulated as a potential marker for assessment of radiation-induced white matter injury (20). A few studies have examined DKI measures in the perilesional white matter (pWM) as compared to

cNAWM, with Delgado et al. finding that the largest changes between grade II and grade III glioma subjects were found with the radial kurtosis (RK) (22), and Eubig et al. showed that RK changes were 4-fold larger as compared to MD in cNAWM of patients with high-grade gliomas as compared to meningiomas (23).

Although changes in cNAWM or pWM in the presence of high-grade gliomas have been reported, these changes are sparsely reported in LGGs. In this study, the value of kurtosis metrics was compared to that of diffusion metrics in identifying changes in solid tumor regions, pWM, and cNAWM in LGGs.

METHODS

Participants

Patients with histologically confirmed World Health Organization (WHO) graded LGGs were recruited for this study. Exclusion criteria included the presence of MRI incompatible metallic objects in the field-of-view and intolerance to gadolinium-based contrast agents. For comparative analysis, healthy normal control (NC) subjects were recruited from the local community. NC subjects completed a self-reporting questionnaire to indicate the absence of neurological or psychological disease or injury and all MRIs were confirmed to be without any structural abnormalities via visual inspection. Informed consent was acquired from each subject and the protocol was approved by the human subjects' research review boards.

MR Imaging Protocol

Subjects underwent a MR imaging protocol at 3T (Siemens Medical Solutions, Erlangen, Germany) comprising of pre- and post-contrast enhanced T1-Weighted (T1WI) magnetization-prepared rapid gradient-echo (MPRAGE) (TR/TE/TI = 2300/2.41/930 ms, resolution = 0.9×0.9×0.7 or 1×1×1 mm^3, flip angle = 9°), FLAIR (TR/TE = 9000/106 ms, resolution = 0.36×0.36×3 mm^3, flip angle = 120°), T2-weighted (TR/TE = 4810/76 ms, resolution = 0.45×0.45×3 mm^3, flip angle = 160°), and DTI/DKI acquired with TR/TE of 6300/99 ms, FOV of 222×222×156 mm, matrix size of 148×148, BW of 1438 Hz/pixel, and a resolution 1.5×1.5×3 mm^3. Diffusion-sensitizing gradient encoding with diffusion weighting factor of b=1000 and 2000 s/mm^2 was applied in 30 directions along with 9 averages for b=0 s/mm^2 (B0).

Image Processing

DKI data were processed using Diffusional Kurtosis Estimator (www.nitrc.org/projects/dke) (24) following skull-stripping using the Brain Extraction Toolbox (FSL 4.0, www.fmrib.ox.ac.uk/fsl) (25). The conventional diffusion measures were calculated by using the data obtained for b = 1000 s/mm^2. Diffusion maps were corrected for geometric distortion using Advanced Normalization Tools diffeomorphic registration tool (26) by registration of the averaged B0 image to the T2-weighted images. Maps for the mean, axial and radial diffusivity (MD, $AD_{,}$ and RD) and FA, and DKI maps of mean, axial and radial kurtosis (MK, $AK_{,}$ and RK) were evaluated for the study. All DTI and DKI maps were registered to the pre-contrast T1 image using a rigid registration (27).

Volumes of interest (VOIs) were semi-automatically drawn in the solid region of the tumor using MIM Maestro™ (www.mimsoftware.com, MIM Software Inc., Cleveland, OH). Initially, VOIs were created on FLAIR images using a Gaussian mixture model to automatically threshold regions of hyperintensity. FLAIR images were segmented using a mixture of three Gaussian distributions and the component with the largest mean value selected as the initial tumor region. Non-tissue regions and cerebrospinal fluid (CSF) were excluded using CSF-labeled segmentation maps derived from T1WI using FSL FAST (28). VOIs were finally edited manually to limit the VOIs to the gross tumor region, which is inclusive of the solid tumor and any surrounding edema. Any enhancing tumor regions seen in post-contrast T1WI MPRAGE images were inherently included in the tumor VOI since enhancement was not seen outside hyperintense FLAIR signal. A VOI for pWM was defined as a 1 cm wide band around the lesion VOI (29,30), limited to the WM.

cNAWM regions were delineated in patients with LGGs and NC using a semi-automatic segmentation approach using T1WI and FLAIR images. Steps included the estimation of the midsagittal plane of the brain on T1WI (31), detection of the contralateral brain hemisphere and delineation of a large contiguous region of WM in the contralateral hemisphere. The contralateral brain hemisphere was identified as the hemisphere of the brain with a larger WM volume. Tissue classification on T1WI images using FAST generally classifies tumor regions as GM, rendering a higher WM volume on the contralateral side of the lesion. Finally, the cNAWM volume was selected as a contiguous WM region in the supraventricular region of the brain (top 6 cm of the brain). All cNAWM regions were visually verified. In Figure 1a the steps of the semi-automatic algorithm for delineating the cNAWM are shown with cNAWM segmented in an example glioma subject (Figure 1b) and in an NC (Figure 1c). In Figure 2 are shown the representative kurtosis and diffusion maps and the generated VOIs for an LGG subject.

Statistical Analysis

Average and standard deviation of MD, MK, AD, RD, AK, RK and FA values were calculated for each VOI in the lesion, pWM, and cNAWM. Shapiro-Wilk test was used to test for normality of the VOI data. General linear models (GLM) with repeated measures were executed and post hoc pairwise comparisons were performed to estimate differences between VOIs of the lesion, pWM, and cNAWM in patients with LGGs. Cohen’s d was calculated to report effect sizes as a measure of sensitivity for the pairwise comparison between two VOIs (32).

Regression analysis was carried out to test the correlation of diffusion and kurtosis measures in the lesion, pWM, and cNAWM in patients with LGGs and cNAWM in NCs to age. Finally, GLMs were used to estimate differences in diffusion and kurtosis metrics in the cNAWM between patients and NCs with age used as a covariate. False Discovery Rate (FDR) corrected p-value of 0.05 was considered significant. For each GLM model, the partial eta-squared was calculated to provide an estimate of the effect size of each diffusion and kurtosis map.

To investigate if the effect sizes derived from counterpart diffusion and kurtosis metrics in the differentiation of VOIs in LGGs and cNAWM between LGGs and NC are significantly

different Cochran's Q test was employed (33). All statistical testing was performed in SPSS version 24 and R.

RESULTS

Nineteen patients (9 females), mean age 48 ± 13 years (Range: 23 to 65 years), with LGGs were recruited for this study. Of the 19 gliomas, there were 9 astrocytomas, 6 oligodendrogliomas, and 3 gangliogliomas with an unconfirmed differentiation for one glioma (male, 47 years). Eight subjects (42%) had received radiochemotherapy prior to imaging with a mean interval of 281 days (Range: 32 to 1478 days) between the end of chemotherapy treatment and imaging. Twenty-six NC subjects (16 females), from age 26 to 60 years (mean age 39 ± 12 years) were recruited for comparative analysis.

Out of the 19 patient studies, 6 subjects (4 astrocytomas, 1 oligodendroglioma, and 1 ganglioglioma) showed enhancement in post-contrast T1WI MPRAGE images. The extracted lesion, pWM, and cNAWM VOIs had an average volume of 40.9 ± 42.6 cc (Range: 1.5 cc to 179.8 cc), 49.2 ± 32.8 cc (Range: 9.0 cc to 108.5 cc), and 43.9 ± 4.9 cc (Range: 32.1 cc to 49.1 cc), respectively. NC subjects enrolled for comparative analysis showed an average volume of 42.5 ± 3.9 cc (Range: 36.5 cc to 49.8 cc) for delineated cNAWM VOIs.

In Figure 3a are shown the average values of MD, MK, AD, RD, AK, RK, and FA for the lesion, pWM, and cNAWM. The Shapiro-Wilk test showed that the data followed a normal distribution for all diffusion and kurtosis metrics in all VOIs (In lesion, AD: $p = 0.722$, MD: $p = 0.156$, RD: $p = 0.467$, FA: $p = 0.071$, AK: $p = 0.521$, MK: $p = 0.180$, RK: $p = 0.058$; In pWM, AD: $p = 0.209$, MD: $p = 0.105$, RD: $p = 0.214$, FA: $p = 0.590$, AK: $p = 0.786$, MK: $p = 0.865$, RK: $p = 0.977$; In cNAWM, AD: $p = 0.224$, MD: $p = 0.222$, RD: $p = 0.319$, FA: $p = 0.638$, AK: $p = 0.678$, MK: $p = 0.262$, RK: $p = 0.879$). Paired analysis showed significant pairwise differences between all VOIs (FDR $p < 0.001$), except for FA maps that failed to show significant differences between lesion and pWM (FDR $p = 0.373$). Diffusivity metrics AD, MD and RD showed a significant ($p < 0.001$) increase in the lesion and pWM compared to cNAWM, whereas kurtosis metrics (AK, MK, and RK) showed a significant ($p < 0.001$) decrease in both the lesion and pWM.

In Figure 3b are shown Cohen's d values for the paired comparisons. For differences between lesions and cNAWM both MD and MK maps show the highest effect sizes, with FA showing the least differences, while for differences between the lesion and surrounding pWM the MK and RK maps showed the highest effect sizes. In discriminating pNAMW and cNAWM, AK maps showed the greatest differences. Comparing corresponding metrics of diffusivity and kurtosis for the mean, axial and radial components, the kurtosis metrics provided a non-significant 0.2% ($Q = 0.01$, $p = 0.985$), 9.0% ($Q = 1.02$, $p = 0.313$), and 0.6% ($Q = 0.01$, $p = 0.955$) increment in effect sizes for distinguishing lesions from cNAWM, respectively. The largest improvement in effect sizes using kurtosis measures over corresponding diffusion measures were obtained in discrimination of the lesion from surrounding pWM, for which kurtosis measures showed a 22.7% ($Q = 3.82$, $p = 0.051$), 29.1% ($Q = 3.96$, $p < 0.05$), and 18.8% ($Q = 2.13$, $p = 0.144$) increase in effect sizes for the mean, axial and radial components respectively, relative to the corresponding diffusion

measures. In contrast, for separation of pWM and cNAWM, the MK and RK showed a 5.2% (Q = 0.32, p = 0.575) and 3.8% (Q = 0.05, p = 0.821) decrement in effect sizes as compared to MD and RD, respectively, whereas AK showed a 25.0% (Q = 6.31, p < 0.05) increase in discriminative power as compared to AD.

The average age of patients with LGGs was found to be significantly higher than NCs (p <0.05). Results of regression with age are shown in Table 1. Regression analysis showed that all diffusion and kurtosis measures, with the exception of FA, in cNAWM of patients with LGGs were significantly correlated with age. In contrast, no significant correlation to age was observed for the VOIs in the lesion or pWM. NCs demonstrated similar age effects as those seen in the cNAWM of patients with LGGs.

Two-tailed t-test showed no significant difference in cNAWM volumes between patients with LGGs and NC (p = 0.2919). Results of the GLM comparison of cNAWM in subjects with LGGs and NCs are shown in Figure 4a. Significant differences between subject groups in cNAWM were seen for FA (FDR p <0.02), MK (FDR p <0.02) and RK maps (FDR p <0.02).

In Figure 4b are shown the effect sizes for diffusion and kurtosis maps in identifying differences in cNAWM of patients with LGGs as compared to NCs. It can be seen that kurtosis maps offer significantly greater differences with RK maps being the most sensitive to differences in cNAWM. MK and RK provide a 587% (Q = 26.29, p < 0.001) and 320% (Q = 12.91, p < 0.001) larger effect size than MD and RD, respectively.

DISCUSSION

This study evaluated the relative performance of diffusion and kurtosis metrics derived from DKI/DWI imaging towards discriminating the tumor and surrounding regions in LGGs and investigated changes of these imaging measures in the cNAWM as compared to normal subjects. The results indicate that kurtosis maps have comparable performance for discrimination of regions of the LGGs as compared to conventional diffusion maps, but considerably greater sensitivity in assessing differences in cNAWM of subjects with LGGs as compared to NCs.

Significant differences were observed for all studied diffusion measures between values in the lesion and those from pWM and cNAWM, with MK and RK showing some advantage for discrimination of the lesion from the surrounding pWM. All kurtosis metrics showed a progressive increase in kurtosis metrics obtained from the solid lesion, pWM, and cNAWM. This finding, also observed in other studies, can be attributed to the lower cellularity accompanied by large cellular sizes resulting in a reduced extracellular space in the tumor region (11,13,22). The resultant structural complexity in the lesion is thus lower than that of cNAWM resulting in increased diffusion metrics accompanied by decreased kurtosis metrics in the lesion as compared to contralateral white matter regions. In addition to the solid region, the pWM also showed decreased kurtosis metrics than the surrounding white matter regions. This is consistent with the study of Delgado et al. that showed significant differences in DKI metrics from the pWM as compared to cNAWM in a mixed group of 35

patients with grade II and III lesions (22). The result shows that tumorigenesis effects in LGGs are seen in surrounding WM regions, which has been demonstrated using histologic studies (14).

This study showed mean, radial and axial kurtosis metrics to be more sensitive to diffuse changes in the pWM with larger effect sizes than corresponding diffusion metrics in delineating the pWM from lesion tissue, whereas AK provided the largest increase in effect size in discriminating pWM from cNAWM. This is contrary to the finding reported by Delgado et al. that showed no significant differences in AK between pWM and cNAWM (22). The discrepancy may be due to the heterogeneity in gliomas induced by the amalgamation of grade II and III gliomas in their study, which included 23 grades II and 12 grade III gliomas. Additionally, Li et al showed that MK was significantly higher in the tumor periphery as compared to the tumor center (consistent with findings in this study) and showed the highest sensitivity in detecting microstructural changes in patients (34). This finding was also demonstrated in this study where MK was found to be the most sensitive parameter for differences between the lesion and the pWM.

A progressive increase in kurtosis metrics was seen in measurements obtained from the solid lesion, pWM, and cNAWM. This progressive trend denotes the fact that LGGs have the lowest cellularity and largest cellular sizes and therefore provide the fewest diffusion barriers, whereas cNAWM with its highly organized structure contains more diffusion barriers (12).

Correlation analysis with age demonstrated that a significant association was found between age and diffusion and kurtosis metrics in the cNAWM. Diffusion metrics have shown to be highly correlated to age (35), but kurtosis measures have shown to demonstrate mixed effects in variations with age (36). On the contrary, both diffusion and kurtosis metrics showed no correlation with age in either of the VOIs of the lesion or the pWM which can be attributed to dysregulation in the vicinity of the lesion.

Few studies have reported changes in the cNAWM of subjects with LGGs. Studies have shown disruptions in the NAWM with DTI (18–21), but DKI changes in the NAWM for LGGs have been less studied. Eubig et al. showed that RK images showed a 4-fold larger change in cNAWM of high-grade glioma patients as compared to subjects with meningiomas, and showed that RK images were the most sensitive in identifying infiltrative effects of high-grade gliomas (23). The findings in this study are consistent with those found by Eubig et al. showing RK to be the most sensitive parameter towards studying abnormalities in cNAWM. In contrast, Van Cauter et al. found no significant differences in non-age-corrected parameter values in the cNAWM between LGG and high-grade glioma patients (13) and did not report age-corrected values in the cNAWM. In this study, age was found to be significantly correlated to diffusion and kurtosis measures in the cNAWM and inclusion of age in the statistical model may have contributed to highlighting differences in cNAWM using RK and MK.

In this study, kurtosis metrics showed 3 to 6 times larger effect sizes in examining changes in cNAWM as compared to their counterpart diffusion metrics, a finding not previously

reported to the best of our knowledge in LGGs. The significant decrease in MK in NAWM of LGG patients, which is regarded as a sign of decreased microstructural complexity, can be attributed to increased water content due to underlying inflammation, demyelination, or axonal disorganization. The accompanying decrease in RK in the cNAWM of LGG patients suggests microstructural disruptions to the cellular membrane or demyelination rather than axonal degeneration indicated by a non-significant increment of AK (37).

The relative sensitivity of diffusion and kurtosis metrics were found to be different across all comparisons made in the study. For example, FA was found to be the least sensitive in identifying changes between the lesion and cNAWM and between the pWM and cNAWM but was found to be highly sensitive in identifying differences between the cNAWM of patients with LGGs and NCs. This finding can be attributed to the complexity in the interpretation of FA, which is affected by various factors including axonal density, the degree of myelination, and fiber organization and orientation (38). FA is often considered a direct marker of white matter integrity, but this is an over-simplification (39). Generally, FA values are reduced in the lesion and surrounding pWM, as also seen in this study. However, tumorigenesis effects in LGGs and surrounding pWM may affect one or more of the underlying factors that affect FA that can result in slightly increased apparent FA (e.g. crossing fibers) and result in a lower sensitivity of FA in identifying changes in the lesion and pWM as compared to cNAWM. On the other hand, more specific perpendicular and parallel components of diffusion and kurtosis can be useful to isolate factors affecting the anisotropy which can be as a result of changes due to inflammation, demyelination, or axonal disorganization. This was seen in the study where AK showed increased sensitivity than RK for identifying changes in lesion and pWM as compared to cNAWM, but RK showed highest differences in cNAWM between patients and controls. This shows that in the vicinity of the lesion, tumorigenesis results in axonal degeneration but primarily affect cellular membrane or demyelination in cNAWM.

Limitations of this study include that the measurements were based on VOIs defined using the FLAIR images in the gross tumor region and may not include the whole tumor environment if it is not visible on FLAIR images, possibly introducing a selection bias. Furthermore, the imaging measures were averaged across a VOI, without regard to possible heterogeneity with the tumor. An additional limitation is the relatively small number of subjects, which meant that potential age-related influences on parameter estimation could be present; although to ameliorate age effects this study did use age as a covariate in GLM analysis. Another limitation that is a consequence of the small sample size is the inability perform a separate analysis of the enhancing regions of the tumor (only 6 subjects with enhancement) limiting the analysis to the gross tumor region. Finally, radiotherapy has shown to induce changes in the microstructural environment (20) and isolating the effects due to radiation treatment and primary gliosis are difficult given the nature of the subject group.

In conclusions, the study showed that kurtosis metrics have comparable performance in the discrimination of regions of the LGGs as compared to conventional diffusion metrics, with kurtosis measures providing a slight advantage for discrimination of the lesion from the surrounding pWM. In addition, kurtosis measures offer considerably greater sensitivity (3–6

fold) in assessing the differences in the cNAWM of subjects with LGGs as compared to normal subjects.

Acknowledgments

Grant Support: This work was supported by National Institute of Health (NIH) grants R01CA172210 and R01EB016064.

Abbreviations Key

DKI	Diffusion Kurtosis Imaging
MK	Mean kurtosis
AK	Axial kurtosis
RK	Radial Kurtosis
FA	Fractional Anisotropy
MD	Mean diffusivity
AD	Axial diffusivity
RD	Radial diffusivity
cNAWM	Contralateral Normal Appearing White Matter
pWM	perilesional White Matter
LGG	Low-grade glioma
NC	normal controls
GLM	General linear model

References

1. Le Bihan D, Breton E, Lallemand D, Grenier P, Cabanis E, Laval-Jeantet M. MR imaging of intravoxel incoherent motions: application to diffusion and perfusion in neurologic disorders. Radiology. 1986; 161:401–407. [PubMed: 3763909]
2. Basser PJ, Mattiello J, LeBihan D. MR diffusion tensor spectroscopy and imaging. Biophys J. 1994; 66:259–267. [PubMed: 8130344]
3. Assaf Y, Cohen Y. Non-mono-exponential attenuation of water and N-acetyl aspartate signals due to diffusion in brain tissue. J Magn Reson. 1998; 131:69–85. [PubMed: 9533908]
4. Jensen JH, Helpern JA, Ramani A, Lu H, Kaczynski K. Diffusional kurtosis imaging: the quantification of non-gaussian water diffusion by means of magnetic resonance imaging. Magn Reson Med. 2005; 53:1432–1440. [PubMed: 15906300]
5. Lu H, Jensen JH, Ramani A, Helpern JA. Three-dimensional characterization of non-gaussian water diffusion in humans using diffusion kurtosis imaging. NMR Biomed. 2006; 19:236–247. [PubMed: 16521095]
6. Fieremans E, Jensen JH, Helpern JA. White matter characterization with diffusional kurtosis imaging. Neuroimage. 2011; 58:177–188. [PubMed: 21699989]
7. Hui ES, Fieremans E, Jensen JH, et al. Stroke assessment with diffusional kurtosis imaging. Stroke. 2012; 43:2968–2973. [PubMed: 22933581]

8. Grossman EJ, Ge Y, Jensen JH, et al. Thalamus and Cognitive Impairment in Mild Traumatic Brain Injury: A Diffusional Kurtosis Imaging Study. J Neurotraum. 2012; 29:2318–2327.
9. Falangola MF, Jensen JH, Tabesh A, et al. Non-Gaussian diffusion MRI assessment of brain microstructure in mild cognitive impairment and Alzheimer's disease. Magn Reson Imaging. 2013; 31:840–846. [PubMed: 23602730]
10. Wang JJ, Lin WY, Lu CS, et al. Parkinson disease: diagnostic utility of diffusion kurtosis imaging. Radiology. 2011; 261:210–217. [PubMed: 21771952]
11. Jiang RF, Jiang JJ, Zhao LY, et al. Diffusion kurtosis imaging can efficiently assess the glioma grade and cellular proliferation. Oncotarget. 2015; 6:42380–42393. [PubMed: 26544514]
12. Raab P, Hattingen E, Franz K, Zanella FE, Lanfermann H. Cerebral gliomas: diffusional kurtosis imaging analysis of microstructural differences. Radiology. 2010; 254:876–881. [PubMed: 20089718]
13. Van Cauter S, Veraart J, Sijbers J, et al. Gliomas: diffusion kurtosis MR imaging in grading. Radiology. 2012; 263:492–501. [PubMed: 22403168]
14. Pallud J, Varlet P, Devaux B, et al. Diffuse low-grade oligodendrogliomas extend beyond MRI-defined abnormalities. Neurology. 2010; 74:1724–1731. [PubMed: 20498440]
15. Price SJ, Jena R, Burnet NG, et al. Improved delineation of glioma margins and regions of infiltration with the use of diffusion tensor imaging: An image-guided biopsy study. Am J Neuroradiol. 2006; 27:1969–1974. [PubMed: 17032877]
16. Giese A, Bjerkvig R, Berens ME, Westphal M. Cost of Migration: Invasion of Malignant Gliomas and Implications for Treatment. J Clin Oncol. 2003; 21:1624–1636. [PubMed: 12697889]
17. Essig M, Giesel F, Stieltjes B, Weber MA. Functional imaging for brain tumors (perfusion, DTI and MR spectroscopy). Radiologe. 2007; 47:513–519. [PubMed: 17505814]
18. Kallenberg K, Goldmann T, Menke J, et al. Abnormalities in the normal appearing white matter of the cerebral hemisphere contralateral to a malignant brain tumor detected by diffusion tensor imaging. Folia Neuropathol. 2014; 52:226–233. [PubMed: 25310733]
19. Horvath A, Perlaki G, Toth A, et al. Increased diffusion in the normal appearing white matter of brain tumor patients: is this just tumor infiltration? J Neuro-Oncol. 2016; 127:83–90.
20. Nagesh V, Tsien CI, Chenevert TL, et al. Radiation-induced changes in normal-appearing white matter in patients with cerebral tumors: a diffusion tensor imaging study. Int J Radiat Oncol Biol Phys. 2008; 70:1002–1010. [PubMed: 18313524]
21. Maudsley AA, Roy B, Gupta RK, et al. Association of metabolite concentrations and water diffusivity in normal appearing brain tissue with glioma grade. J Neuroimaging. 2014; 24:585–589. [PubMed: 24251857]
22. Delgado Anna F, Fahlström M, Nilsson M, et al. Diffusion kurtosis imaging of gliomas grades II and III - a study of perilesional tumor infiltration, tumor grades and subtypes at clinical presentation. Radiol Oncol. 2017; 51:121. [PubMed: 28740446]
23. Eubig J, Patil V, Johnson G. Diffusion Kurtosis MRI of Normal Appearing White Matter in Glioma Patients. Radiological Society of North America 2011 Scientific Assembly and Annual Meeting; Chicago IL. 2011;
24. Tabesh A, Jensen JH, Ardekani BA, Helpern JA. Estimation of tensors and tensor-derived measures in diffusional kurtosis imaging. Magn Reson Med. 2011; 65:1507–1507.
25. Smith SM, Jenkinson M, Woolrich MW, et al. Advances in functional and structural MR image analysis and implementation as FSL. Neuroimage. 2004; 23(Suppl 1):S208–219. [PubMed: 15501092]
26. Avants BB, Epstein CL, Grossman M, Gee JC. Symmetric diffeomorphic image registration with cross-correlation: Evaluating automated labeling of elderly and neurodegenerative brain. Med Image Anal. 2008; 12:26–41. [PubMed: 17659998]
27. Studholme C, Hill DLG, Hawkes DJ. An overlap invariant entropy measure of 3D medical image alignment. Pattern Recogn. 1999; 32:71–86.
28. Zhang Y, Brady M, Smith S. Segmentation of brain MR images through a hidden Markov random field model and the expectation-maximization algorithm. IEEE T Med Imaging. 2001; 20:45–57.

29. Mourad AF, Mohammad HE-dG, Sayed MM, Ragae MA. What's the clinical significance of adding diffusion and perfusion MRI in the differentiation of glioblastoma multiforme and solitary brain metastasis? The Egyptian Journal of Radiology and Nuclear Medicine. 2017; 48:661–669.
30. Tsougos I, Svolos P, Kousi E, et al. Differentiation of glioblastoma multiforme from metastatic brain tumor using proton magnetic resonance spectroscopy, diffusion and perfusion metrics at 3 T. Cancer Imaging. 2012; 12:423–436. [PubMed: 23108208]
31. Jayasuriya SA, Liew AWC. Symmetry plane detection in neuroimages based on intensity profile analysis. 2012 International Symposium on Information Technologies in Medicine and Education (ITME 2012); 2012. 599–603.
32. Falangola MF, Guilfoyle DN, Tabesh A, et al. Histological correlation of diffusional kurtosis and white matter modeling metrics in cuprizone-induced corpus callosum demyelination. NMR Biomed. 2014; 27:948–957. [PubMed: 24890981]
33. Cochran WG. The Combination of Estimates from Different Experiments. Biometrics. 1954; 10:101–129.
34. Li F, Shi W, Wang D, et al. Evaluation of histopathological changes in the microstructure at the center and periphery of glioma tumors using diffusional kurtosis imaging. Clin Neurol Neurosur. 2016; 151:120–127.
35. Cauter SV, Veraart J, Sijbers J, et al. Gliomas: Diffusion Kurtosis MR Imaging in Grading. Radiology. 2012; 263:492–501. [PubMed: 22403168]
36. Lätt J, Nilsson M, Wirestam R, et al. Regional Values of Diffusional Kurtosis Estimates in the Healthy Brain. J Magn Reson Imaging. 2013; 37:610–618. [PubMed: 23055442]
37. Marrale M, Collura G, Brai M, et al. Physics, Techniques and Review of Neuroradiological Applications of Diffusion Kurtosis Imaging (DKI). Clin Neuroradiol. 2016; 26:391–403. [PubMed: 26589207]
38. Winston GP. The physical and biological basis of quantitative parameters derived from diffusion MRI. Quant Imaging Med Surg. 2012; 2:254–265. [PubMed: 23289085]
39. Jones DK, Knosche TR, Turner R. White matter integrity, fiber count, and other fallacies: the do's and don'ts of diffusion MRI. Neuroimage. 2013; 73:239–254. [PubMed: 22846632]

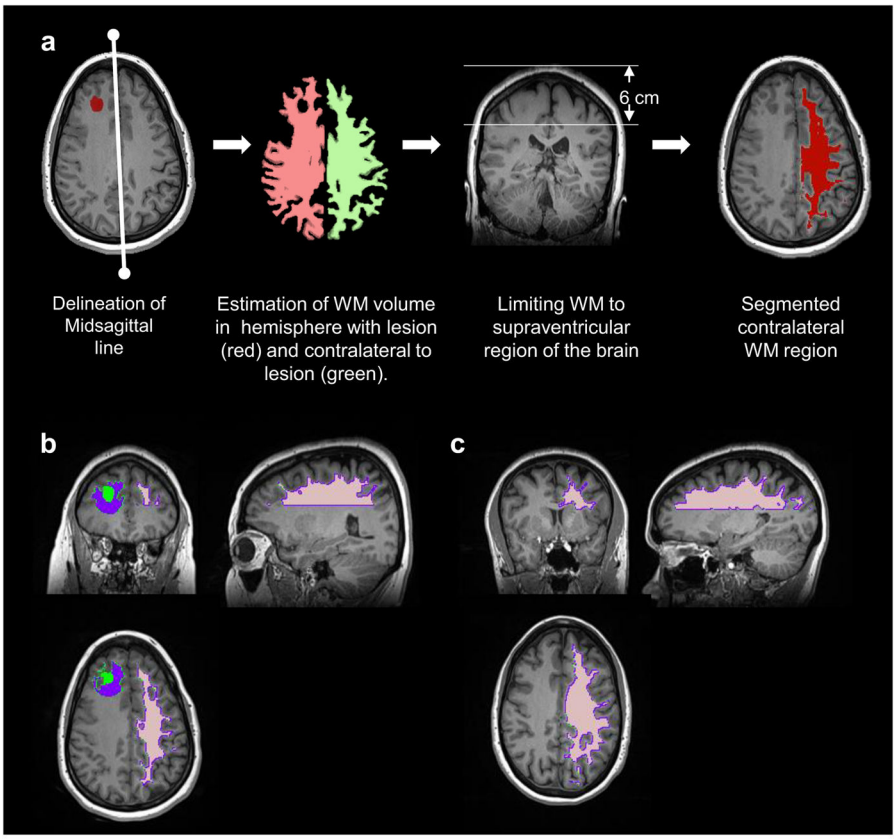

Figure 1.

a) Steps used for the semi-automatic algorithm for delineating the cNAWM. b) Example extracted cNAWM (shown in pink) with the lesion (green) and perilesional white matter (pWM) (purple) shown in a 46-year-old female with astrocytoma. c) Example extracted cNAWM (pink) in a healthy control.

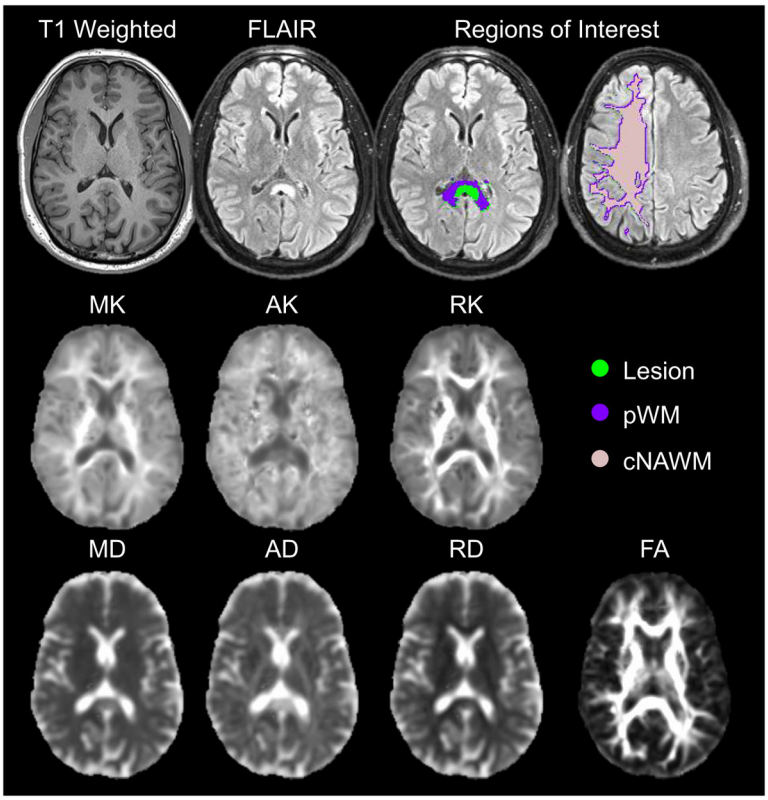

Figure 2.

Example structural T1-weighted and FLAIR images; the studied region of interests in the lesion (green), perilesional white matter (pWM) (purple), and contralateral normal appearing white matter (cNAWM) (pink); kurtosis maps of mean kurtosis (MK), axial kurtosis (AK) and radial kurtosis (RK); diffusion maps for mean diffusion (MD), axial diffusion (AD) and radial diffusion (RD); and fractional anisotropy (FA) for a 46-year-old male with oligodendroglioma.

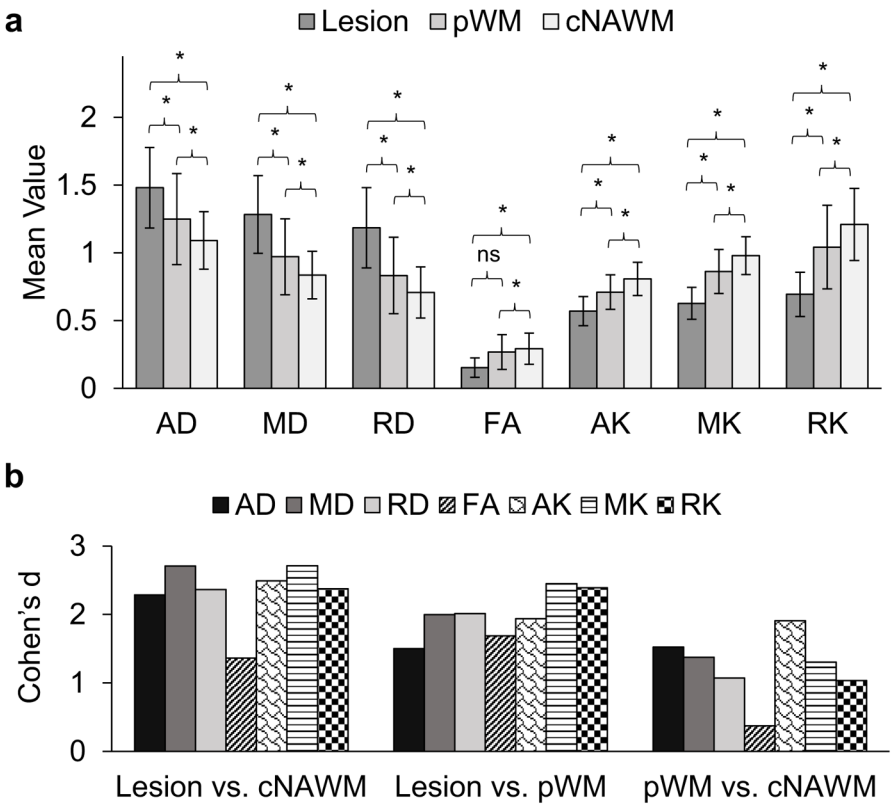

Figure 3.

a) Average values for mean, axial and radial diffusivity (MD, AD, and RD) and kurtosis (MK, AK, and RK) and fractional anisotropy (FA) in the solid lesion, surrounding perilesional white matter (pWM) and contralateral normal appearing white matter (cNAWM) in 19 patients with low-grade gliomas. Mean, axial and radial diffusivity have units 10^{-3} mm^2/sec; mean, axial and radial kurtosis and fractional anisotropy are dimensionless. The significance of paired differences are shown by * denoting False Discovery Rate (FDR) corrected p <0.001. b) Effect size calculated using Cohen's *d* for paired differences.

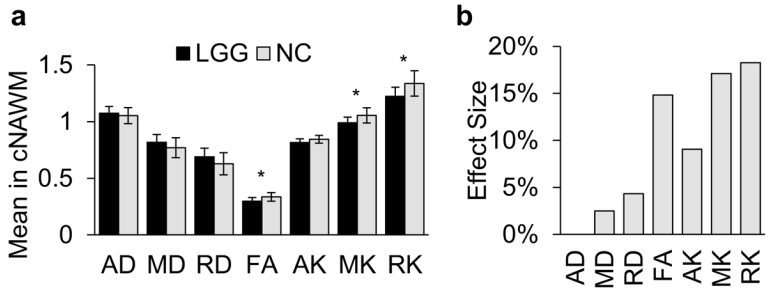

Figure 4.

a) Average values for mean, axial and radial diffusivity (MD, AD, and RD) and kurtosis (MK, AK, and RK) and fractional anisotropy (FA) in contralateral normal appearing white matter (cNAWM) patients with low grade gliomas (LGG) and normal controls (NC). Mean, axial and radial diffusivity have units 10^{-3} mm^2/sec; mean, axial and radial kurtosis and fractional anisotropy are dimensionless. The significance of general linear model (GLM) analysis is shown by * denoting False Discovery Rate (FDR) corrected $p < 0.05$. b) Effect size calculated using partial eta-squared for GLM.

Table 1

Correlation of mean diffusion and kurtosis metrics to age in the lesion, pWM, and cNAWM of patients with LGGs and in cNAWM of normal controls.

	Low Grade Gliomas R^2 (FDR p-value)		Normal Controls R^2 (FDR p-value)	
	Lesion	**cNAWM**	**IPR**	**cNAWM**
AD	0.01 (0.287)	*0.46 (<0.05)*	0.07 (0.138)	*0.42 (<0.05)*
MD	0.01 (0.253)	*0.39 (<0.05)*	0.18 (0.061)	*0.41 (<0.05)*
RD	0.01 (0.260)	*0.34 (<0.05)*	0.22 (0.053)	*0.32 (<0.05)*
FA	0.01 (0.258)	0.18 (0.059)	0.09 (0.115)	0.17 (0.062)
AK	0.10 (0.117)	*0.35 (<0.05)*	0.03 (0.206)	*0.29 (<0.05)*
MK	0.10 (0.111)	*0.25 (<0.05)*	0.01 (0.277)	*0.26 (<0.05)*
RK	0.06 (0.148)	*0.23 (<0.05)*	0.01 (0.293)	*0.25 (<0.05)*

† Significant correlations after FDR multiple corrections are italicized.